Theor Chem Acc (2011) 128:127–136
DOI 10.1007/s00214-010-0783-x

REGULAR ARTICLE

Assessment of the ωB97 family for excited-state calculations

Denis Jacquemin · Eric A. Perpète · Ilaria Ciofini · Carlo Adamo

Received: 1 June 2010 / Accepted: 6 July 2010 / Published online: 20 July 2010

Abstract We benchmark three recently proposed range-separated hybrids, namely ωB97, ωB97X and ωB97XD in the framework of time-dependent density functional theory simulations of electronic absorption spectra. Comparisons are made with both theoretical estimates obtained by highly correlated approaches and experimental wavelengths of maximal absorption measured for important classes of $\pi \rightarrow \pi^*$ and $n \rightarrow \pi^*$ chromogens. The amplitude of the errors induced by the lack of vibronic coupling in our computational model is also evaluated for five dyes. The performances of the ωB97 group are systematically compared to the results of other global and range-separated hybrids. It turns out that ωB97XD provides, in general, more accurate estimates than ωB97X and ωB97.

Keywords TD-DFT · Range-separated hybrids · ωB97 · Benchmarks

1 Introduction

It is now well recognized that hybrid functionals, incorporating a fraction of Hartree-Fock-like (HF) exchange [1], tend to provide more accurate results than pure density functionals for most properties of organic molecules [2]. In that framework, the developments of more refined hybrid functionals have been achieved along several directions [3–6]. Notably, the extension of the standard global hybrids (GH) include the explicit consideration of virtual orbitals (leading to the so-called double-hybrid functionals) [7–9] as well as the development of range-separated approaches [10, 11]. Range-separated hybrids (RSH) use a growing fraction of exact exchange when the inter-electronic distance increases, in such a way that the asymptotical behavior is correctly reproduced when this distance tends to infinity. This procedure originally suggested by Savin, [10–12], has led to the emergence of several series of functionals and we especially want to pinpoint: (1) Hirao's long-range-corrected (LC) functionals [13–15]; (2) Handy's CAM-B3LYP (Coulomb-attenuating method) [16, 17]; (3) Scuseria's LC-ωPBE [18, 19]; (4) Baer's BNL scheme [20]; and (5) Head-Gordon's ωB97 series [21, 22]. RSHs have been tested for several challenging properties, and astonishing successes have been obtained for non-linear optics properties [12, 23–27] and bond length alternations [28, 29] of conjugated oligomers. Computations of the transition energies with the time-dependent DFT (TD-DFT) approach [30, 31]—the focus of the present paper—have also been performed with RSH. The first works of this kind have mainly been devoted to the determination of

Electronic supplementary material The online version of this article (doi:10.1007/s00214-010-0783-x) contains supplementary material, which is available to authorized users.

D. Jacquemin · E. A. Perpète
Groupe de Chimie-Physique Théorique et Structurale,
Facultés Universitaires Notre-Dame de la Paix,
Rue de Bruxelles, 61, 5000 Namur, Belgium
e-mail: denis.jacquemin@fundp.ac.be

I. Ciofini · C. Adamo (✉)
Ecole Nationale Supérieure de Chimie de Paris,
Laboratoire Electrochimie et Chimie Analytique,
UMR CNRS-ENSCP No. 7575, 11, Rue Pierre et Marie Curie,
75321 Paris Cedex 05, France
e-mail: carlo-adamo@enscp.fr

Present Address:
D. Jacquemin (✉)
Laboratoire CEISAM-UMR 6230, 2 Rue de la Houssiniére,
BP 92208, 44322 Nantes Cedex 3, France
e-mail: Denis.Jacquemin@univ-nantes.fr

charge-transfer transitions [15, 18, 21, 32–37], and of Rydberg states in small molecules [14, 20, 38]. In both cases, selecting RSH during the TD-DFT step allowed to obtain accurate estimates. More recently, benchmark calculations have been carried out for less specific excited states, notably by Peach et al. for the CAM-B3LYP functional [39], by Rohrdanz and Herbert with their own approach [40, 41], by Caricato et. al. and by us for LC-DFT, LC-ωPBE and CAM-B3LYP schemes [42–47]. However, to the best of our knowledge, no large-scale investigation aiming at assessing the performances of the ωB97 series in the TD-DFT framework has been proposed yet, and this contribution aims at filling this gap. Nevertheless, we want to point out that it has already been demonstrated that the attenuation parameter influences significantly the relative performance of ωB97 for valence and charge-transfer states [41]. It should also be noticed that the ωB97 [21] ωB97X [21], and ωB97XD [22] functionals have originally been designed for other purposes, but assessing their relative performance w.r.t. other global and range-separated hybrids helps understanding the key parameters necessary to obtain accurate estimates of transition energies.

Following the strategy set up in Refs. [45] and [48], we use two complementary approaches to benchmark the ωB97 series of functionals in the present article. First, we compare TD-DFT results to electron-correlated wave-function estimates, this is the "*versus* theory" (VT) scheme. This procedure allows straightforward (clearly defined vertical states) and coherent (gas-phase, same ground-state geometry and basis set) benchmarks but is inherently limited by the availability of highly accurate reference data. In other words, only small-sized compounds might be considered and this may be a problematic drawback as the TD-DFT errors computed for small systems are not necessary representative of the deviations obtained for larger compounds [45]. As VT set, we have selected the data recently collected by Thiel et al. [49–51]. This set contains a larger number of singlet–singlet and singlet–triplet transitions computed for 28 small molecules (the largest are naphthalene and the DNA bases) at the CC2, CCSD, CC3 and CAS-PT2 levels of approximations. In a second stage, we use several experimental values to benchmark the ωB97 functionals, a strategy referred to as "*versus* experiment" (VE) in the following. In practice, these experimental values are the longest wavelength of maximal absorption (λ_{max}) measured in condensed phase. The VE approach advantageously allows to optimize the agreement with measured data, a common purpose of theoretical chemists. However, several drawbacks emerge, such as the impossibility to exactly mimic experimental conditions (temperature, pressure, complex solvent effects,…) and the difficulty to model the observed transition (we compare vertical transitions to λ_{max}, rather than 0-0 bands in each case). In that sense, the VT and VE approaches can certainly be viewed as complementary.

This paper is organized as follows: in Sect. 2, we present methodological and computational details, in Sect. 3, we explore the performances of the ωB97 set in the VT scheme and Sect. 4 provides a similar analysis in the VE approach.

2 Methodology

All calculations have been performed with Gaussian09 [52]. The three functionals of the ωB97 family have been used: ωB97 [21] ωB97X [21], and ωB97XD [22]. These three RSH are range-separated hybrids, have been build upon the B97 functional [53] and use the error function to split the electron repulsion operator into short-range and long-range terms [10]:

$$\frac{1}{r_{12}} = \frac{\mathrm{erf}(\omega r_{12})}{r_{12}} + \frac{\mathrm{erfc}(\omega r_{12})}{r_{12}} \quad (1)$$

where ω is the damping parameter controlling the rate of growth of the exact exchange when the r_{12} increases. Though there are several parameters in these three functionals (see Refs. [21] and [22]), we underline that their DFT/HF mixing varies. First, they rely on substantially different damping parameter: 0.4 bohr^{-1} for ωB97, 0.3 bohr^{-1} for ωB97X and 0.2 bohr^{-1} for ωB97XD. Second, they do not use the same amount of short-range exact exchange. In ωB97, like in most RSH, there is no short-range exchange, whereas in ωB97X and ωB97XD, this short-range exchange percentage attains 15.77 and 22.20%, respectively. In other words, in this family, there is an equilibrium between the amount of short-range exact exchange and the damping parameter. For comparison purposes, we mainly selected two other RSH, namely Vydrov and Scuseria's LC-ωPBE that uses $\omega = 0.40$ a.u. and no short-range exchange [18, 19] and CAM-B3LYP that presents a ω of 0.33 a.u. and 19% of short-range exchange [16]. A specificity of CAM-B3LYP is that the HF-like exchange does not tend to 100% but to 65%, when r_{12} tends to infinity.

2.1 Small molecules: the VT set

Aiming at fully consistent comparisons with the values reported by the group of Thiel [49, 50], we have used the same MP2/6-31G(d) geometries and TZVP basis set during the TD-DFT calculations. The VT set is divided into two subgroups: 103 singlet–singlet excited states and 63 singlet–triplet transitions. For all 168 cases, "theoretical best estimates" (TBE) are available in Ref. [50]. The same or

similar sets have been previously used by us [45, 47, 48] and by others [50, 54] to benchmark DFT functionals and semi-empirical methods [55]. Nevertheless, a series of clarifications are necessary: (1) the TBE are not strictly obtained in the same theoretical conditions so that we have also selected the CAS-PT2/TZVP (singlets) and CC3/TZVP (triplets) results listed in Ref. [50] to benchmark the ωB97 functionals. This choice is justified as these two approaches are found to be respectively efficient for these subsets [49]. (2) The selection of the same atomic basis set (TZVP) for both TD-DFT and reference values ensures consistency but this diffuse-less basis does not yield converged results for all states. However, we have recently shown, for the triplet subset, that the selection of much more extended basis sets, such as 6-311++G(3df,3pd) or *aug*-cc-pVTZ, might modify the conclusions for a few specific states but induces negligible alterations on the statistical data [47]. A detailed discussion of basis set effects for the CC reference values can be found elsewhere [56]. (3) While the TBE, CAS-PT2 and CC3 values cannot be viewed as perfectly accounting for all electron correlation effects, they are plausibly close enough to the theoretical limit for vertical gas-phase transitions and we assume that the errors solely originate from the DFT functionals.

2.2 Large molecules: the VE set

For the VE set, we have followed a well-established methodology [57], which was already selected in our most recent benchmarks [43–45]. In this approach, the ground-state geometries are first optimized with PBE0 [3, 58] using the 6-311G(d,p) basis set. Such procedure provides accurate structural parameters [59] and allows straightforward comparisons with our previous assessments [45, 48]. It is also noticeable that using a RSH for both the optimization of the geometry and excited state does not lead to better performances in most cases [40, 44]. Following this first stage, the vibrational frequencies have been determined to check the absence of imaginary frequency. In the last step, the vertical transition energies are estimated with the standard vertical TD-DFT/6-311+G(2d,p) procedure. At each three stages, the bulk solvent effects have been included through the polarizable continuum model (PCM) [60, 61], using a linear-response non-equilibrium scheme for the TD-DFT calculations [62].

In this VE set, we have included typical molecular dyes (see Fig. 1) encompassing different types of transitions ($n \rightarrow \pi^*/\pi \rightarrow \pi^*$, charge-transfer/localized). We have also investigated representative examples of two classes of photochromes, namely diarylethenes and spirooxazines, considering in both cases their most delocalized forms. As noted in the Introduction, we compare vertical transitions to experimental λ_{max}, an unphysical approximation. The errors induced by this approach are certainly non-negligible [63–65] but computing the vibronic coupling for a large set of real-life molecules in solvated environments is beyond reasonable computational reach. Therefore, we have also compared vertical TD-DFT estimates to experimental values corrected for vibronic effects. Such procedure has been recently proposed [54, 66], and is applied here on a set of five molecules (**MG-1** to **MG-5**, Fig. 1), in an effort to estimate if the use of a vertical model might lead to bogus conclusions. In Ref. [54], the experimental 0-0 values are corrected for solvent effects (calculated at the PBE0/6-31G(d) level) and vibronic contributions (evaluated at the PBE/TZVP level), so as to yield reference figures for gas-phase vertical results. In a second step, vertical TD-DFT/TZVP calculations are used to benchmark a large panel of functionals [54]. Here, we applied our VE methodology: the structures provided in Ref. [54] have been re-optimized at the PCM-PBE0/6-311G(d,p) level and vertical PCM-TD-DFT/6-311+G(2d,p) excited states have been subsequently determined. In other words, the experimental data have not been corrected for medium effects, that are already included in our approach, and only the vibronic corrections are taken from Ref. [54].

3 VT benchmarks

Tables S1 and S2 in supporting information collate all transition energies computed with the ωB97, ωB97X and ωB97XD functionals for the singlet and the triplet states of the VT set, respectively. Error patterns obtained for both families of transitions can be found in Fig. 2. The performances of pure density functionals [45, 47, 48, 50], global hybrids [45, 47, 48, 50], range-separated hybrids [45, 47] as well as double hybrids [54] for simulating the excitation energies of "chemical" subsets of molecules of the VT set are already well discussed in the literature. Therefore, we focus our analysis on statistical trends allowing to assess the relative accuracy of the three ωB97 functionals. This analysis can be found in Table 1 that reports mean signed errors (MSE, reference minus TD-DFT values), mean absolute errors (MAE), root mean square deviations (RMS) as well as the square of the linear correlation coefficients (R^2) obtained through least-square fits. This last parameter allows to gauge the relative consistency of several functionals. In Table 1, it is obvious that the average errors obtained by considering the TBE or the CAS-PT2/CC3 references are akin so that we only discuss the former below.

For singlets, all three ωB97 functionals tend to significantly overestimate the transition energies but the deviations drop when a smaller ω damping parameter is

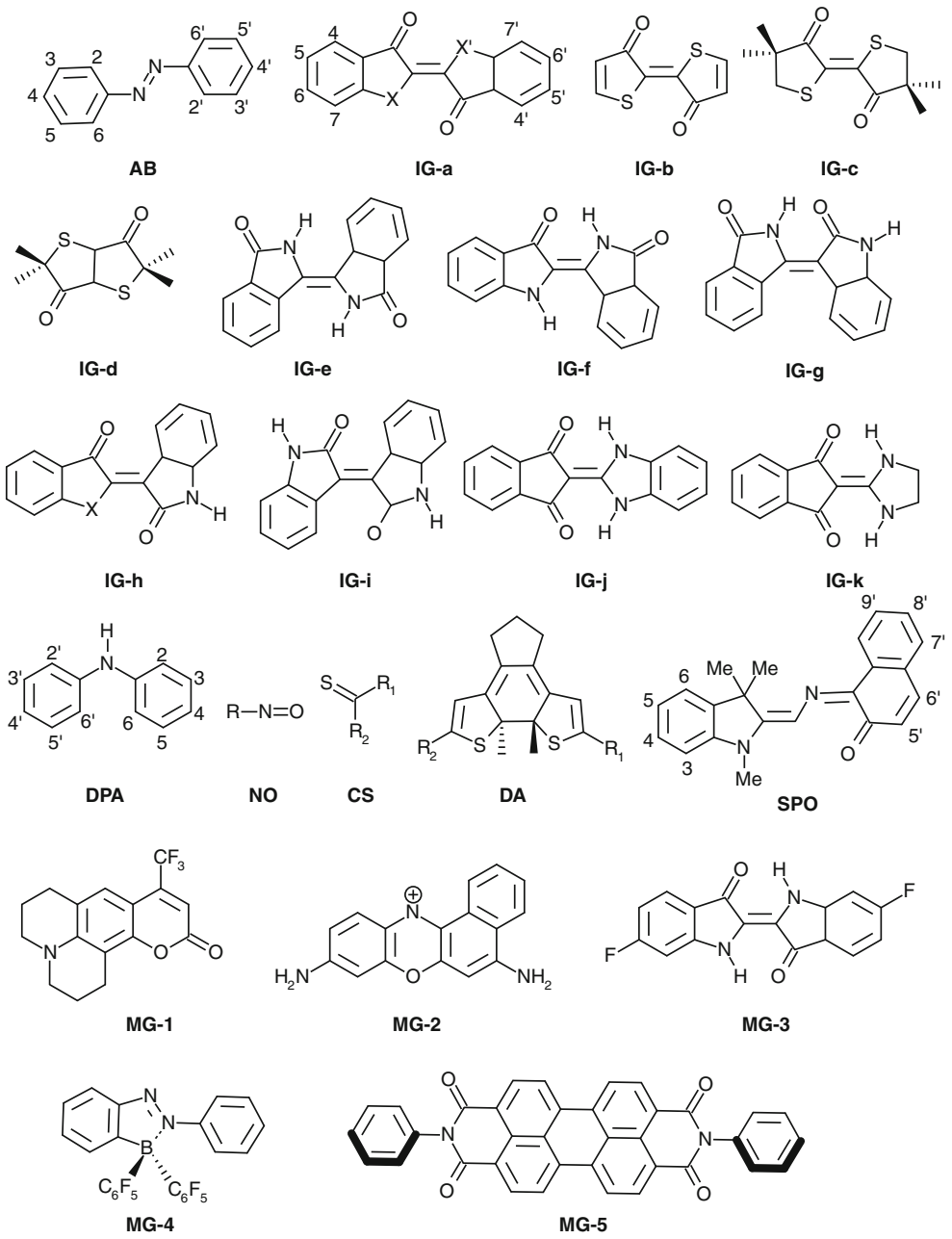

Fig. 1 Sketch of the investigated molecules in the VE set

selected. The dispersion of the errors follows the same trend (see Fig. 2), so that the correlation coefficient is larger for ωB97XD than for ωB97 and ωB97X. Clearly, for singlets, the ωB97XD approach is the most efficient ambassador of his family and delivers a MAE of 0.31 eV, in the line of the expected TD-DFT accuracy [39, 45, 63]. Nevertheless, none of the three tested RSH can outperform B3LYP for any of the four statistical criteria, and the absolute deviations are about twice the one obtained with the more refined B2PLYP approach, the latter standing as the most accurate scheme tested up to now for this singlet VT set [54]. A comparison of the results of all RSH listed in Table 1 shows that ωB97 (ωB97XD) delivers average deviations similar to the one of LC-ωPBE (CAM-B3LYP). The same holds for the raw transitions energies, e.g. for both pairs of RSH, the mean absolute deviations (between their estimates) are limited to 0.04 eV, and the R^2 are very close to 1.0. Eventually, if we consider only the 37 $n \rightarrow \pi^*$ transitions of the singlet VT set, we obtain MAE of 0.41 eV, 0.33 eV and 0.20 eV for ωB97, ωB97X and ωB97XD, respectively. The fact that most functionals tend to provide more accurate estimates for $n \rightarrow \pi^*$ than for

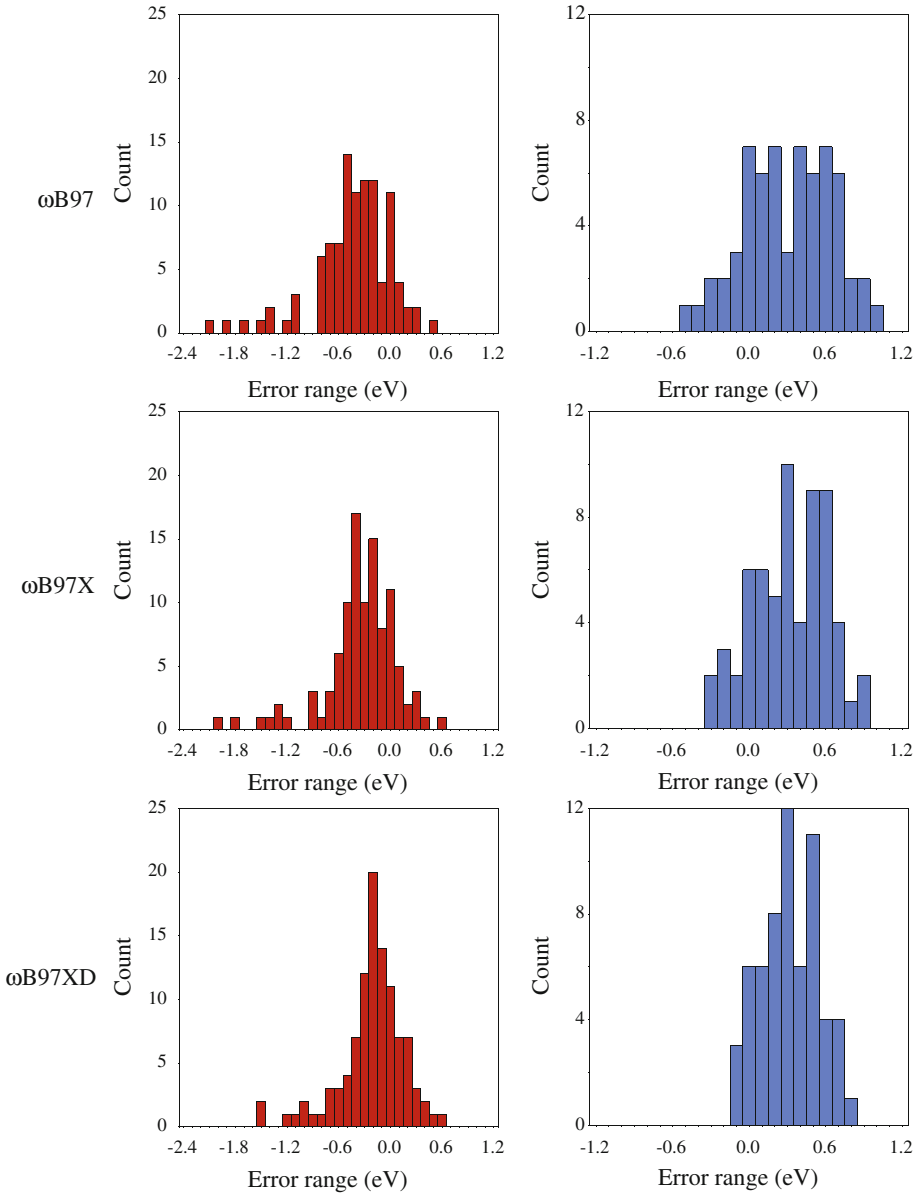

Fig. 2 Error patterns in the VT set: singlets (*left in red*) and triplets (*right in blue*)

$\pi \rightarrow \pi^*$ states has already been recognized [45, 50], and the ωB97 family follows this expected behavior.

If the DFT/HF mixing remains the key parameter for singlet states, it is known that the actual mathematical forms of the exchange and correlation functionals have a large impact for singlet–triplet transitions [47]. In fact, for triplet states, the similarity between, on the one hand, LC-ωPBE and ωB97, and, on the other hand, CAM-B3LYP and ωB97XD does not pertain as the mean absolute deviations computed for their raw values are 0.20 and 0.10 eV, for the two pairs, respectively. From Table 1, it is obvious that the three ωB97 RSH, based on the same B97 foundation, yield relatively similar MSE and MAE, though ωB97XD delivers again the smallest deviations and largest correlation coefficients. Contrary to singlets, TD-ωB97 provide too small singlet–triplet excitation energies. In fact, for triplets, the 0.32 eV MAE of ωB97XD is smaller than any of the ten RSH considered previously [47]. Though two GH, namely BMK (0.24 eV) and M06-2X (0.23 eV) [47], are more accurate than ωB97XD, it is clear from Table 1 that the ωB97 family outperforms both B3LYP and CAM-B3LYP, a significant achievement.

In short, for the VT set, ωB97XD emerges as the most efficient functional of its family. If comparisons are performed with respect to previously benchmarked functionals, one notes that ωB97XD yields average performances for singlet states (that are often overestimated) and relatively accurate estimates for triplet states (that tend to be underestimated).

Table 1 Statistical analysis of the performances of several DFT functionals for the VT set, using the TBE values of Ref. [50] as reference

Functional	Singlet excited states				
	MSE	MAE	RMS	R^2	Ref.
BP86	0.44	0.52	0.62	0.92	[50]
B3LYP	0.07	0.27	0.33	0.94	[50]
M06	0.12 (0.16)	0.28 (0.31)	0.34 (0.38)	0.95 (0.95)	[48]
BHandHLYP	−0.43	0.50	0.62	0.89	[50]
M06-2X	−0.23 (−0.18)	0.34 (0.35)	0.46 (0.46)	0.92 (0.92)	[48]
B2LYP	0.45	0.52	0.62	0.90	[54]
B2PLYP	0.01	0.18	0.25	0.97	[54]
ωB97	−0.43 (−0.39)	0.47 (0.45)	0.62 (0.60)	0.90 (0.89)	This work
ωB97X	−0.35 (−0.31)	0.40 (0.39)	0.55 (0.53)	0.91 (0.90)	This work
ωB97XD	−0.21 (−0.17)	0.31 (0.30)	0.43 (0.42)	0.93 (0.92)	This work
LC-ωPBE	−0.41 (−0.36)	0.46 (0.45)	0.61 (0.60)	0.90 (0.89)	[45]
CAM-B3LYP	−0.22 (−0.18)	0.31 (0.30)	0.42 (0.41)	0.93 (0.93)	[45]
DFT/MR-CI	0.13	0.22	0.29	0.96	[50]
Functional	Triplet excited states				
	MSE	MAE	RMS	R^2	Ref.
BP86	0.53	0.53	0.61	0.94	[50]
B3LYP	0.45	0.45	0.49	0.98	[50]
M06	0.44 (0.48)	0.44 (0.48)	0.47 (0.51)	0.98 (0.98)	[47]
BHandHLYP	0.55	0.60	0.76	0.88	[50]
M06-2X	0.07 (0.11)	0.23 (0.23)	0.28 (0.29)	0.94 (0.96)	[47]
ωB97	0.29 (0.34)	0.38 (0.40)	0.45 (0.49)	0.95 (0.95)	This work
ωB97X	0.31 (0.35)	0.35 (0.39)	0.38 (0.46)	0.96 (0.96)	This work
ωB97XD	0.31 (0.35)	0.32 (0.30)	0.36 (0.41)	0.98 (0.98)	This work
LC-ωPBE	0.50 (0.54)	0.55 (0.57)	0.66 (0.70)	0.93 (0.93)	[47]
CAM-B3LYP	0.41 (0.45)	0.42 (0.45)	0.48 (0.51)	0.97 (0.97)	[47]
DFT/MR-CI	0.24	0.25	0.28	0.99	[50]

The values between brackets correspond to CAS-PT2/TZVP (singlets) or CC3/TZVP (triplets) benchmarks for the same series of states, see Tables S1 and S2. The MSE, MAE and RMS are in eV. R^2 is the square of the linear correlation coefficient. Note that the values listed for B2LYP ad B2PLYP have been recalculated from the data of Ref. [54], so to use the same reference values

4 VE benchmarks

The full VE set (Fig. 1) has been divided into three subsets: $\pi \rightarrow \pi^*$ dyes, $n \rightarrow \pi^*$ chromogens and photochromes. In the first subset, three important families of organic dyes have been considered, namely azobenzenes (**AB**), indigoïds (**IG**) and nitro-diphenylaniline (**DPA**), all of which have been treated with TD-DFT previously (see Ref. [45] and references therein), therefore allowing consistent comparisons. The computed transition energies for these three kinds of chromophores can be found in Tables S3–S5 in Supporting Information, whereas Table 2 collates the statistical values. In the **IG** series, the transitions mostly present a local nature [67], whereas they imply a significant charge-transfer in **DPA** [68]. For **AB**, the character of the visible band is guided by the electronic donor/acceptor strength of the substituents. All three members of the ωB97 group tend to overestimate the transition energies, and the extend of this error is proportional to the amplitude of the damping parameter. Indeed, as can be seen in Fig. 3, the most probable errors are −0.5, −0.4 and −0.3 eV for ωB97, ωB97X and ωB97XD, respectively. As already noted in the VT set, the errors obtained with ωB97 and LC-ωPBE are completely similar, though, in the present case, larger differences between the ωB97XD and CAM-B3LYP are detected. This finding is related to the size of the molecules investigated in the VE set: the amount of exact exchange at large inter-electronic distance (that differs for ωB97XD and CAM-B3LYP) becomes an important parameter for medium-size parameters. These two RSH both surpass B3LYP and PBE0 for azobenzenes but provide poorer estimates for indigoïds (MAE of 0.32 eV with

Table 2 Statistical analysis of the performances of ωB97 functionals in computing $\pi \rightarrow \pi^*$ transitions in three families of organic dyes

Functional	AB			
	MSE	MAE	RMS	R^2
B3LYP	0.27	0.29	0.32	0.91
PBE0	0.16	0.20	0.23	0.93
ωB97	−0.40	0.40	0.44	0.93
ωB97X	−0.32	0.32	0.37	0.95
ωB97XD	−0.17	0.19	0.25	0.95
LC-ωPBE	−0.40	0.40	0.44	0.93
CAM-B3LYP	−0.11	0.16	0.20	0.94
Functional	IG			
	MSE	MAE	RMS	R^2
B3LYP	0.04	0.10	0.13	0.95
PBE0	−0.04	0.10	0.13	0.96
ωB97	−0.58	0.58	0.59	0.97
ωB97X	−0.45	0.46	0.47	0.98
ωB97XD	−0.32	0.32	0.34	0.97
LC-ωPBE	−0.54	0.54	0.55	0.97
CAM-B3LYP	−0.29	0.29	0.31	0.98
Functional	DPA			
	MSE	MAE	RMS	R^2
B3LYP	0.18	0.18	0.20	0.96
PBE0	0.02	0.06	0.08	0.96
ωB97	−0.63	0.63	0.64	0.92
ωB97X	−0.53	0.53	0.54	0.92
ωB97XD	−0.34	0.34	0.35	0.93
LC-ωPBE	−0.60	0.60	0.61	0.92
CAM-B3LYP	−0.24	0.24	0.26	0.94
Functional	AB+IG+DPA			
	MSE	MAE	RMS	R^2
B3LYP	0.16	0.20	0.24	0.92
PBE0	0.06	0.14	0.17	0.93
ωB97	−0.51	0.51	0.54	0.93
ωB97X	−0.40	0.41	0.44	0.93
ωB97XD	−0.26	0.27	0.31	0.93
LC-ωPBE	−0.49	0.49	0.51	0.93
CAM-B3LYP	−0.20	0.23	0.26	0.94

For comparisons, the B3LYP, PBE0, LC-ωPBE and CAM-B3LYP values, computed for the same set of molecules from the data listed in Ref. [45], are added

ωB97XD) and for diphenylaniline derivatives (MAE of 0.34 eV with ωB97XD). For the latter charge-transfer dyes, the accuracy obtained with B3LYP, and especially PBE0, might look surprising but can be explained by the non-zero overlap between the relevant occupied and virtual orbitals [68]. Indeed, in that case, Peach et. al. have shown that GH are adequate [39]. Among the three functionals, only ωB97XD can be considered as satisfying for simulating low-lying $\pi \rightarrow \pi^*$ states, as it leads to a MAE close to the 0.3 eV threshold for each families. On top of that, we stress that this functional provides a 0.19 eV average error and a promising correlation coefficient for azobenzenes, the most preeminent class of industrial dyes (ca. 60% of the world production of organic dyes).

For $n \rightarrow \pi^*$ transitions, we have considered two kinds chromogens presenting a large separation between the dipole-forbidden and dipole-allowed bands, namely nitroso (**NO**) and thiocarbonyl (**CS**) dyes. The raw data can be found in Tables S6 and S7, whereas statistical values can be found in Table 3 and Fig. 3. For the three functionals, the most probable error is close to 0.0 eV (Fig. 3) and this success can mainly be ascribed to nitroso dyes for which the ωB97 family provides very accurate estimates, as do the majority of GH and RSH [42, 45]. For thiocarbonyls, all hybrid functionals overestimate the transition energies, though the errors are still relatively small and the correlation with experimental reference is excellent. For $n \rightarrow \pi^*$ transitions, the most efficient functional of the ωB97 group remains ωB97XD that behaves similar to CAM-B3LYP.

The position of the absorption bands of photochromes are given in Tables S8 and S9, and the average errors are listed in Table 4. For diarylethenes, ωB97XD appears extremely powerful with MSE limited to −0.01 eV and a MAE as small as 0.03 eV. CAM-B3LYP also provides accurate values for this class of molecular switches, [43, 69], that present a highly delocalized excited state. For spirooxazines, the deviations are much larger (close to 0.4 eV for the three RSH) and the correlation coefficients are notably poorer than for any of the other molecular sets. This problem, common to all (TD-)DFT schemes [70], probably originates from the merocyanine nature of open **SPO**. Indeed, for cyanine-like molecules, a single determinantal approach is bond to fail [71], and not even the most refined hybrids can overcome this difficulty [9, 20].

In Table 5, we report the transition energies for the set of **MG-x** dyes recently proposed by Grimme et al. [54]. For **MG-4**, pure density functionals have a tendency to yield spurious states [54], and the three ωB97 hybrids cure the problem and deliver a first excited state with a large oscillator strength ($f > 0.3$) and a dominant HOMO/LUMO character. From 5, it is clear that the ωB97 functionals still overestimate the transition energies, but to a smaller extend than in the vertical approximation, for similar $\pi \rightarrow \pi^*$ states. In any case, ωB97XD clearly remains the most efficient: it yields the smallest deviations in all but one (**MG-2**) case. For comparisons, the M06 (M06-2X) GH provides a MSE of 0.11 (−0.13) eV and a MAE of 0.18 (0.14) eV for the same set of molecules [48]. Therefore,

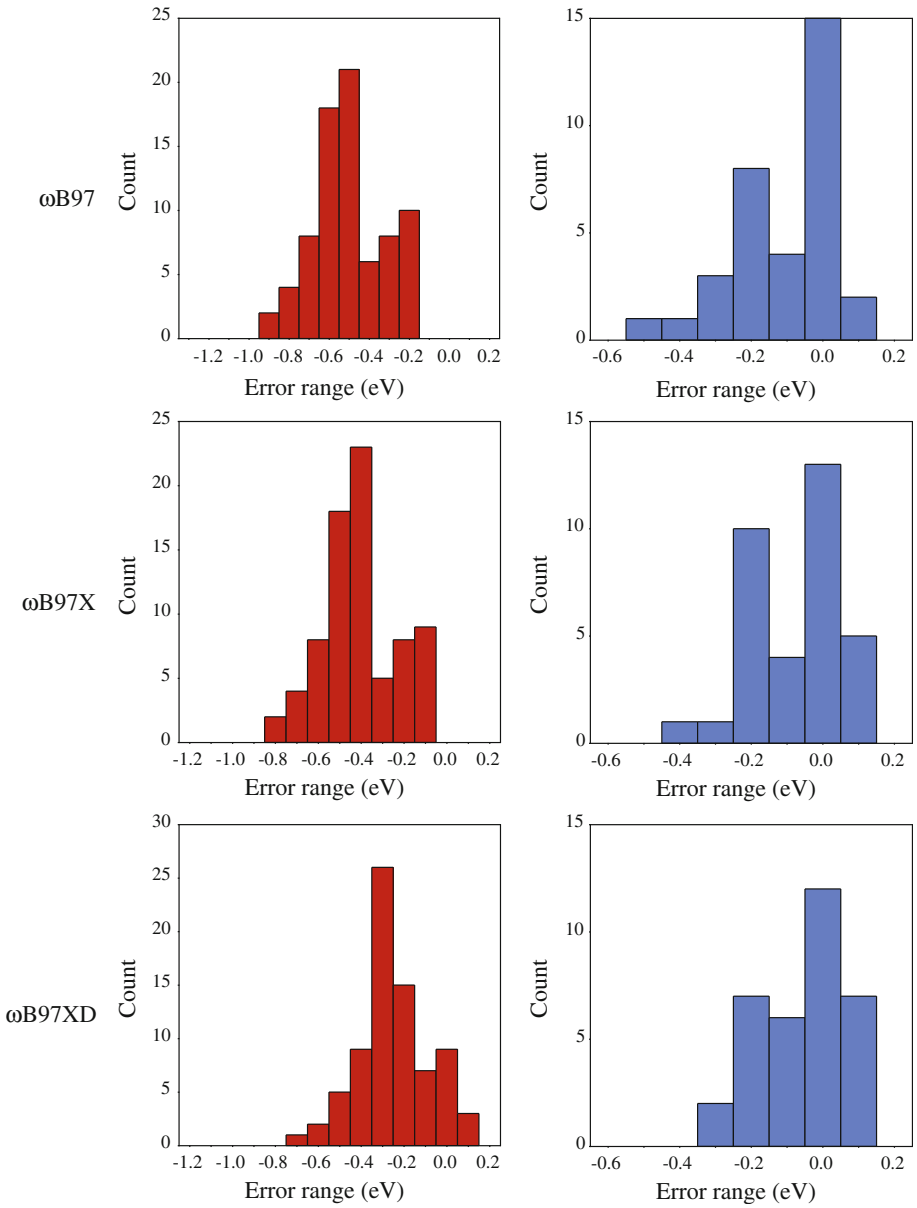

Fig. 3 Error patterns in the VE set: $\pi \rightarrow \pi^*$ transitions (AB+IG+DPA, *left in red*) and $n \rightarrow \pi^*$ transitions (NO+CS, *right in blue*)

Table 3 Statistical analysis of the performances of ωB97 functionals in computing $n \rightarrow \pi^*$ transitions

Functional	NO				CS				NO+CS			
	MSE	MAE	RMS	R^2	MSE	MAE	RMS	R^2	MSE	MAE	RMS	R^2
B3LYP	0.02	0.06	0.08	0.99	−0.09	0.10	0.11	0.99	−0.03	0.08	0.10	0.99
PBE0	0.03	0.08	0.09	0.99	−0.16	0.16	0.17	0.99	−0.06	0.11	0.14	0.99
ωB97	−0.02	0.05	0.07	0.99	−0.21	0.21	0.25	0.99	−0.11	0.13	0.18	0.99
ωB97X	0.00	0.05	0.07	0.99	−0.17	0.17	0.20	0.99	−0.08	0.11	0.15	0.99
ωB97XD	0.01	0.06	0.07	0.99	−0.14	0.14	0.16	0.99	−0.06	0.10	0.12	0.99
LC-ωPBE	0.05	0.08	0.09	0.99	−0.16	0.17	0.21	0.99	−0.05	0.12	0.16	0.99
CAM-B3LYP	0.01	0.05	0.07	0.99	−0.13	0.13	0.15	0.99	−0.05	0.09	0.12	0.99

See caption of Table 2 for more details

Table 4 Statistical analysis of the performances of ωB97 functionals in computing the λ_{max} of photochromes. See caption of Table 2 for more details

Functional	DA				SPO				DA+SPO			
	MSE	MAE	RMS	R^2	MSE	MAE	RMS	R^2	MSE	MAE	RMS	R^2
ωB97	−0.27	0.27	0.27	0.95	−0.43	0.43	0.43	0.79	−0.36	0.36	0.37	0.85
ωB97X	−0.17	0.17	0.17	0.95	−0.41	0.41	0.42	0.76	−0.31	0.31	0.32	0.63
ωB97XD	−0.01	0.03	0.04	0.96	−0.37	0.37	0.37	0.67	−0.21	0.22	0.28	0.24

Table 5 Benchmark calculations for the five **MG** dyes

Dye	ωB97	ωB97X	ωB97XD	0−0	VC	Vert
MG-1	3.78	3.71	3.56	2.95	0.41	3.36
MG-2	2.60	2.59	2.56	2.02	0.24	2.26
MG-3	2.71	2.64	2.52	2.12	0.26	2.38
MG-4	3.46	3.38	3.25	2.72	0.35	3.07
MG-5	2.78	2.71	2.58	2.33	0.24	2.57
MSE	−0.34	−0.28	−0.17			
MAE	0.34	0.28	0.17			
RMS	0.35	0.29	0.19			
R^2	0.99	0.98	0.95			

The experimental 0-0 values as well as the theoretical vibronic corrections (VC) are taken in Ref. [54] and used to determine the vertical values for the experimental results. All results are in eV

once vibronic effects have been accounted for, the performance discrepancies of ωB97XD and these two *meta*-GGA hybrids become relatively small.

5 Conclusion

The performances of three range-separated functionals build upon the B97 functional, namely ωB97, ωB97X and ωB97XD, have been assessed for the calculation of low-lying excited-state energies. Two series of benchmarks have been considered (*versus* theory and *versus* experiment) and they lead to consistent tendencies. Indeed, the three functionals yield too large transition energies in most cases, at the notable exception of the $n \rightarrow \pi^*$ nitroso dyes and singlet–triplet transition energies (that are underestimated). For singlet states, ωB97 behaves like LC-ωPBE and the ωB97XD results are often similar to their CAM-B3LYP counterparts.

For the nearly 300 transitions listed in this work, the mean absolute deviations are 0.41, 0.36 and 0.27 eV for ωB97, ωB97X and ωB97XD, respectively. Therefore, it is clear that ωB97XD provides the most accurate estimates of this family of RSH and this is consistent with the smaller damping parameter used [40, 41]. This conclusion holds for all sets of molecules, transitions and both the VT and VE benchmarks. More specifically, ωB97XD is very efficient for azobenzene dyes and diarylethene photochromes, two essential families of organic conjugated molecules. For the other families treated herein, ωB97XD provides errors larger than the one obtained with typical global hybrids, such as B3LYP or PBE0, at least within the vertical approximation. In that framework, ωB97XD provides on average more accurate values than LC-ωPBE but is slightly less efficient than CAM-B3LYP. Once vibronic effects are taken into account, the ωB97 functionals still overestimate the transition energies but to a lesser extend. This investigation therefore supports recent TD-DFT benchmarks performed on large dyes that have shown that depending on the approximation (vertical or not), different conclusions could be reached regarding the optimal amount of exact exchange [45, 66].

Acknowledgments DJ and EAP thank the Belgian National Fund for Scientific Research for their research associate and senior research associate positions, respectively. Several calculations have been performed on the Interuniversity Scientific Computing Facility (ISCF), installed at the Facultés Universitaires Notre-Dame de la Paix (Namur, Belgium), for which the authors gratefully acknowledge the financial support of the FNRS-FRFC and the "Loterie Nationale" for the convention number 2.4578.02 and of the FUNDP. The collaboration between the Belgian and French groups is supported by the *Wallonie-Bruxelles International*, the *Fonds de la Recherche Scientfique*, the *Ministère Français des Affaires étragères et européennes*, the *Ministère de l'Enseignement supérieur et de la Recherche* in the framework of Hubert Curien Partnership.

References

1. Becke AD (1993) J Chem Phys 98:5648
2. Perdew JP, Ruzsinszky A, Constantin LA, Sun J, Csonka GI (2009) J Chem Theory Comput 5:902
3. Adamo C, Barone V (1999) J Chem Phys 110:6158
4. Boese AD, Martin JML (2004) J Chem Phys 121:3405
5. Zhao Y, Schultz NE, Truhlar DG (2006) J Chem Theory Comput 2:364
6. Zhao Y, Truhlar DG (2008) Acc Chem Res 41:157
7. Grimme S (2006) J Chem Phys 124:034108
8. Schwabe T, Grimme S (2006) Phys Chem Chem Phys 8:4398
9. Grimme S, Neese F (2007) J Chem Phys 127:154116
10. Savin A (1966) In: Seminario JM (eds) Recent developments and applications of modern density functional theory, Chap 9. Elsevier, Amsterdam, pp 327–354
11. Leininger T, Stoll H, Werner HJ, Savin A (1997) Chem Phys Lett 275:151

12. Toulouse J, Colonna F, Savin A (2004) Phys Rev A 70:062505
13. Iikura H, Tsuneda T, Yanai T, Hirao K (2001) J Chem Phys 115:3540
14. Tawada T, Tsuneda T, Yanagisawa S, Yanai T, Hirao K (2004) J Chem Phys 120:8425
15. Chiba M, Tsuneda T, Hirao K (2006) J Chem Phys 124:144106
16. Yanai T, Tew DP, Handy NC (2004) Chem Phys Lett 393:51
17. Yanai T, Harrison RJ, Handy NC (2005) Mol Phys 103:413
18. Vydrov OA, Scuseria GE (2006) J Chem Phys 125:234109
19. Vydrov OA, Heyd J, Krukau V, Scuseria GE (2006) J Chem Phys 125:074106
20. Livshits E, Baer R (2007) Phys Chem Chem Phys 9:2932
21. Chai JD, Head-Gordon M (2008) J Chem Phys 128:084106
22. Chai JD, Head-Gordon M (2008) Phys Chem Chem Phys 10:6615
23. Sekino H, Maeda Y, Kamiya M (2005) Mol Phys 103:2183
24. Kamiya M, Sekino H, Tsuneda T, Hirao K (2005) J Chem Phys 122:234111
25. Jacquemin D, Perpète EA, Medved' M, Scalmani G, Frisch MJ, Kobayashi R, Adamo C (2007) J Chem Phys 126:191108
26. Jacquemin D, Perpète EA, Ciofini I, Adamo C (2008) J Comput Chem 29:921
27. Kishi R, Bonness S, Yoneda K, Takahashi H, Nakano M, Botek E, Champagne B, Kubo T, Kamada K, Ohta K, Tsuneda T (2010) J Chem Phys 132:094107
28. Jacquemin D, Perpète EA, Scalmani G, Frisch MJ, Kobayashi R, Adamo C (2007) J Chem Phys 126:144105
29. Peach MJG, Tellgren E, Salek P, Helgaker T, Tozer DJ (2007) J Phys Chem A 111:11930
30. Runge E, Gross EKU (1984) Phys Rev Lett 52:997
31. Casida ME (1995) Dsgr. In: Chong DP (ed) Time-dependent density-functional response theory for molecules, volume 1 of Recent advances in density functional methods. World Scientific, Singapore, pp 155–192
32. Rudberg E, Salek P, Helgaker T, Agren H (2005) J Chem Phys 123:184108
33. Cai ZL, Crossley MJ, Reimers JR, Kobayashi R, Amos RD (2006) J Phys Chem B 110:15624
34. Kobayashi R, Amos RD (2006) Chem Phys Lett 420:106
35. Lange AW, Rohrdanz MA, Herbert JM (2008) J Phys Chem B 112:6304
36. Jensen L, Govind N (2009) J Phys Chem A 113:9761
37. Aittala PJ, Cramariuc O, Hukka TI (2010) J Chem Theory Comput 6:805
38. Peach MJG, Cohen AJ, Tozer DJ (2006) Phys Chem Chem Phys 8:4543
39. Peach MJG, Benfield P, Helgaker T, Tozer DJ (2008) J Chem Phys 128:044118
40. Rohrdanz MA, Herbert JM (2008) J Chem Phys 129:034107
41. Rohrdanz MA, Martins KM, Herbert JM (2009) J Chem Phys 130:054112
42. Jacquemin D, Perpète EA, Vydrov OA, Scuseria GE, Adamo C (2007) J Chem Phys 127:094102
43. Jacquemin D, Perpète EA, Scuseria GE, Ciofini I, Adamo C (2008) J Chem Theory Comput 4:123
44. Jacquemin D, Perpète EA, Scuseria GE, Ciofini I, Adamo C (2008) Chem Phys Lett 465:226
45. Jacquemin D, Wathelet V, Perpète EA, Adamo C (2009) J Chem Theory Comput 5:2420
46. Caricato M, Trucks GW, Frisch MJ, Wiberg KB (2010) J Chem Theory Comput 6:370
47. Jacquemin D, Perpète EA, Ciofini I, Adamo C (2010) J Chem Theory Comput 6:1532
48. Jacquemin D, Perpète EA, Ciofini I, Adamo C, Valero R, Zhao Y, DG Truhlar (2010) J Chem Theory Comput 6:2071
49. Schreiber M, Silva-Junior MR, Sauer SPA, Thiel W (2008) J Chem Phys 128:134110
50. Silva-Junior MR, Schreiber M, Sauer SPA, Thiel W (2008) J Chem Phys 129:104103
51. Sauer SPA, Schreiber M, Silva-Junior MR, Thiel W (2009) J Chem Theory Comput 5:555
52. Frisch MJ, Trucks GW, Schlegel HB, Scuseria GE, Robb MA, Cheeseman JR, Scalmani G, Barone V, Mennucci B, Petersson GA, Nakatsuji H, Caricato M, Li X, Hratchian HP, Izmaylov AF, Bloino J, Zheng G, Sonnenberg JL, Hada M, Ehara M, Toyota K, Fukuda R, Hasegawa J, Ishida M, Nakajima T, Honda Y, Kitao O, Nakai H, Vreven T, Montgomery JA Jr, Peralta JE, Ogliaro F, Bearpark M, Heyd JJ, Brothers E, Kudin KN, Staroverov VN, Kobayashi R, Normand J, Raghavachari K, Rendell A, Burant JC, Iyengar SS, Tomasi J, Cossi M, Rega N, Millam JM, Klene M, Knox JE, Cross JB, Bakken V, Adamo C, Jaramillo J, Gomperts R, Stratmann RE, Yazyev O, Austin AJ, Cammi R, Pomelli C, Ochterski JW, Martin RL, Morokuma K, Zakrzewski VG, Voth GA, Salvador P, Dannenberg JJ, Dapprich S, Daniels AD, Farkas O, Foresman JB, Ortiz JV, Cioslowski J, Fox DJ (2009) Gaussian 09 Revision A.02, Gaussian Inc., Wallingford CT
53. Becke AD (1997) J Chem Phys 107:8544
54. Goerigk L, Moellmann J, Grimme S (2009) Phys Chem Chem Phys 11:4611
55. Silva-Junior MR, Thiel W (2010) J Chem Theory Comput 6:1546
56. Silva-Junior MR, Sauer SPA, Schreiber M, Thiel W (2010) Mol Phys 108:453
57. Jacquemin D, Perpète EA, Ciofini I, Adamo C (2009) Acc Chem Res 42:326
58. Ernzerhof M, Scuseria GE (1999) J Chem Phys 110:5029
59. Adamo C, Scuseria GE, Barone V (1999) J Chem Phys 111:2889
60. Tomasi J, Mennucci B, Cammi R (2005) Chem Rev 105:2999
61. For the records, the reader should be aware that the details of the PCM parameters (UAKS/UA0 radii, presence/absence of smoothing spheres...) might vary from one family of dye to the other
62. Cossi R, Barone V (2001) J Chem Phys 115:4708
63. Dierksen M, Grimme S (2004) J Phys Chem A 108:10225
64. Santoro F, Improta R, Lami A, Bloino J, Barone V (2007) J Chem Phys 126:184102
65. Jacquemin D, Peltier C, Ciofini I (2010) Chem Phys Lett 493:67
66. Goerigk L, Grimme S (2010) J Chem Phys 132:184103
67. Jacquemin D, Preat J, Wathelet V, Fontaine M, Perpète EA (2006) J Am Chem Soc 128:2072
68. Jacquemin D, Bouhy M, Perpète EA (2006) J Chem Phys 124:204321
69. Jacquemin D, Michaux C, Perpète EA, Maurel F, Perrier A (2010) Chem Phys Lett 488:193
70. Perrier A, Maurel F, Perpète EA, Wathelet V, Jacquemin D (2009) J Phys Chem A 113:13004
71. Schreiber M, Bub V, Fülscher MP (2001) Phys Chem Chem Phys 3:3906